On three-dimensional singular stress/residual stress fields at the front of a crack/anticrack in an orthotropic/orthorhombic plate under anti-plane shear loading

Reaz A. Chaudhuri [*]

Department of Materials Science and Engineering, 122 S. Central Campus Dr., Room 304, University of Utah, Salt lake City, UT 84112-0560, United States

ABSTRACT

A novel eigenfunction expansion technique, based in part on separation of the thickness-variable, is developed to derive three-dimensional asymptotic stress field in the vicinity of the front of a semi-infinite through-thickness crack/anticrack weakening/reinforcing an infinite orthotropic/orthorhombic plate, of finite thickness and subjected to far-field anti-plane shear loading. Crack/anticrack-face boundary conditions and those that are prescribed on the top and bottom (free, fixed and lubricated) surfaces of the orthotropic plate are exactly satisfied. Five different through-thickness crack/anticrack-face boundary conditions are considered: (i) slit crack, (ii) anticrack or perfectly bonded rigid inclusion, (iii) transversely rigid inclusion (longitudinal slip permitted), (iv) rigid inclusion in part perfectly bonded, the remainder with slip, and (v) rigid inclusion located alongside a crack. Explicit expressions for the singular stress fields in the vicinity of the fronts of the through-thickness cracks, anticracks or mixed crack–anticrack type discontinuities, weakening/reinforcing orthotropic/orthorhombic plates, subjected to far-field anti-plane shear (mode III) loadings, are presented. In addition, singular residual stress fields in the vicinity of the fronts of these cracks, anticracks and similar discontinuities are also discussed.

© 2009 Elsevier Ltd. All rights reserved.

1. Introduction

Asymptotic behavior of two-dimensional stress fields at the tips of cracks, anticracks and homogeneous/bimaterial wedges, has been studied extensively in the literature [1–4]. An anticrack is a rigid (line in two-dimension, planar in three-dimension) inclusion, and is essentially a through slit crack filled with an infinitely rigid lamella, which unlike a crack transmits tractions, but prevents a displacement discontinuity. A rigid lamella may be in the form of a single crystal layer, or an atomic hydrogen layer diffused into metallic lattice or grain boundary. More likely scenario may, however, involve reaction products that are often brittle ceramic compounds, formed at high temperatures during the processing of metal matrix composites. Anticracks have important applications in the field of materials science, because they can be idealized representations of manufacturing defects such as embrittlements (e.g., hydrogen embrittlement) or ceramic reaction products, and are as much a source of materials failure as cracks. As regards hydrogen embrittlement, it is presently believed by materials scientists that molecular hydrogen is dissociated by a chemisorption process, which allows the liberated atomic hydrogen to diffuse internally into the metallic lattice and grain boundary thus forming an embrittled layer [5]. Atomic hydrogen can diffuse rapidly through a metal lattice, because its size is smaller than the lattice parameter [5]. The first objective of the present investigation is to solve the crack and anticrack problems of orthotropic materials, such as fiber reinforced composites and orthorhombic single crystals, from a three-dimensional perspective. Discovery of superconductivity in La–Ba–Cu–O system in the1980s by Bednorz and Muller (1987 Nobel laureates in Physics) had spurred an enormous amount of interests in such monocrystalline perovskite type oxides as the oxygen deficient $YBa_2Cu_3O_x$, which are of orthorhombic symmetry [6]. However, practical applications of such monocrystalline superconductors are restricted at cryogenic temperature by their poor fracture toughness and associated mechanical characteristics [6].

Another issue of great concern to designers of orthotropic materials, such as orthorhombic single crystals and fiber reinforced composites, is the residual stress. For example, the presence of residual stresses in silicon single crystals (cubic, being a special case of orthotropic materials) greatly affects the performance and reliability of the integrated circuits [7]. Residual stresses are developed in silicon wafers during the growth phase as well as in the thermal processing. These stresses can be determined in wafers by analysis of the out-of-plane deformation. A second example relates to the processing (i.e., chemical/thermal)-induced residual stresses in composites, which can be high enough to cause cracking

* Tel.: +1 801 581 6282; fax: +1 801 581 4816.
E-mail address: r.chaudhuri@utah.edu

within the matrix even before mechanical loading is applied [8]. This micro-cracking of the matrix can expose the fibers to degradation by chemical attack. Strength is adversely affected by residual stresses since a pre-loading has been introduced. These residual stresses are nonsingular in nature, i.e., they, when derived or computed by a linear elastic analysis technique, do not "blow up" (or approach infinity) as a crack front is approached. Unfortunately, the problem of residual stress in the context of fracture mechanics has not been addressed in the literature, which is the second objective of the present investigation. This latter type of residual stresses, which are associated with crack/anticrack type discontinuities, do "blow up" at the fronts of these sharp discontinuities, when derived or computed using a methodology based on linear elastic fracture mechanics (LEFM).

A number of numerical methods, such as finite element methods (FEM) and boundary integral equation methods (BIEM), are nowadays widely used, because they can handle arbitrary geometries and complex far-field loadings, that would almost be intractable to any known analytical approach. In the absence of the knowledge of the strength of a singularity, however, in regions where the elastic stresses become unbounded, the majority of weighted residual type methods, such as the FEM, encounter overwhelming numerical problems, such as lack of convergence and oscillation resulting in poor accuracy [9]. Furthermore, as Stenger et al. [9] has observed, for traditional numerical methods such as finite difference, finite element and polynomial methods, the existence of corners drastically decreases the rate of convergence of the solution, and the order of singularity cannot be explicitly computed. Current modifications of these methods introduce special "boundary elements" which mimic the singular behavior of the solution, but, to be able to do this effectively, requires a knowledge of the exact nature of the singularity, which may at times be difficult to deduce for a three-dimensional state of stress.

The mathematical difficulties posed by the three-dimensional crack and anticrack problems are substantially greater than their two-dimensional counterparts. A three-dimensional eigenfunction approach has recently been developed by Chaudhuri and Xie [10], and Chaudhuri [11] for understanding the singular stress behavior in the vicinity of a point located at the front of a crack and an anticrack, respectively. This has been extended to determine the asymptotic stress fields in the neighborhood of points located at the fronts of homogeneous and bimaterial pie-shaped wedges [12], and their special cases of bimaterial interface cracks [13] and free edges [14]. It may also be noted here that the above three-dimensional eigenfunction expansion technique has also been utilized to compute the asymptotic stress fields in the vicinity of fronts of penny shaped cracks/anticracks weakening homogeneous and bimaterial media [15,16], and thus establishing a conceptual similarity of this class of three-dimensional crack problems with their through-thickness counterparts. In addition, the three-dimensional singular stress fields near a partially debonded cylindrical rigid fiber [17], and in the vicinity of the circumferential tip of a fiber–matrix interfacial debond [18,19] have also been derived using the same afore-mentioned three-dimensional eigenfunction expansion technique. The three-dimensional asymptotic stress fields in the vicinity of the line of intersection of a circular cylindrical through/part-through open/rigidly plugged hole [20] as well as an elastic inclusion [21] and a plate has also been derived using the same three-dimensional eigenfunction expansion approach. Finally, an asymptotic solution pertaining to the stress field in the neighborhood of the circumferential line of intersection of an interface of a two-layer plate made of dissimilar isotropic materials and a through-hole, subjected to far-field extension/ bending (mode I), in-plane shear-twisting (mode II) and torsional (mode III) loadings, has also been derived using the same technique [22], which is in agreement with its counterpart

derived by Folias [23], using Lure's symbolic method. This does not only lend credence to the validity of the afore-mentioned three-dimensional eigenfunction expansion approach, but also establishes a conceptual as well as mathematical similarity of the afore-cited four classes of three-dimensional singularity problems.

In regards to the anti-plane shear problems, Ma and Hour [24] have solved the anti-plane problem of two dissimilar anisotropic wedges of arbitrary aperture angles that are bonded together along a common edge, using the Mellin transform technique. More recently, the problems of three-dimensional asymptotic stress fields in the neighborhood of the fronts of bimaterial pie-shaped wedges of symmetric and unsymmetric geometrical configurations (with respect to the bimaterial interface) and subjected to anti-plane shear far-field loading have been solved by Xie and Chaudhuri [25], and Chiu and Chaudhuri [26], respectively. In what follows, a simple, yet novel and hitherto unavailable eigenfunction expansion type method, based on the separation of the thickness-variable technique, is developed in conjunction with the Stroh type affine transformation [1], to obtain three-dimensional asymptotic stress fields in the vicinity of the fronts of semi-infinite through-thickness cracks/anticracks, weakening/reinforcing orthotropic plates subjected to far-field anti-plane shear loading. Section 2 provides a mathematical statement of the problem under investigation. This new three-dimensional eigenfunction expansion method is employed to derive explicit expressions for the three-dimensional asymptotic singular stress fields in the vicinity of points located at the fronts of through-thickness cracks/anticracks, subjected to the five combinations of crack/anticrack-face boundary conditions. Three different boundary conditions, free, fixed and lubricated, are applied on the top and bottom surfaces of the orthotropic/orthorhombic plate. These expressions for the singular stress fields in the vicinity of the crack/anticrack fronts weakening/ reinforcing orthotropic/orthorhombic plates, of finite thickness and subjected to anti-plane shear loading, presented in Section 3, reduce to their isotropic counterparts [10,11].

2. Formulation of the problem

The Cartesian coordinate system (x, y, z) is convenient to describe the deformation behavior in the vicinity of a semi-infinite through-thickness crack/anticrack, weakening/reinforcing an infinite orthotropic plate of thickness, 2 h (Figs. 1 and 2). Here, the z-axis is placed along the straight crack/anticrack front, while the coordinates x, y, are used to define the directions along the length of the crack/anticrack and transverse to it, respectively, in the plane of the plate. u, v and w represent the components of the displacements in the x, y and z directions, respectively. The orthotropic material investigated here is of orthorhombic type with x–y, y–z and x–z planes serving as the three planes of symmetry [27]. In case of continuous fiber reinforced composites, the fibers are placed parallel to x-direction lying on the x–y plane (or z-plane). The present approach can easily be extended to an anisotropic lamina with arbitrary fiber orientation on a plane of symmetry, e.g., x–y plane. Cracks have experimentally been observed to propagate parallel to the fiber directions in a composite lamina. A local x–y–z coordinate system can always be selected to coincide with the fiber direction (x), lateral direction (y) and thickness direction (z).

The three equilibrium equations for a linear elastic solid can be expressed in terms of the displacement components u, v, and w, as follows:

$$c_{11} \frac{\partial^2 u}{\partial x^2} + c_{66} \frac{\partial^2 u}{\partial y^2} + c_{55} \frac{\partial^2 u}{\partial z^2} + (c_{12} + c_{66}) \frac{\partial^2 v}{\partial x \partial y} + (c_{13} + c_{55}) \frac{\partial^2 w}{\partial x \partial z} = 0,$$

$$(1a)$$

$$(c_{12} + c_{66}) \frac{\partial^2 u}{\partial x \partial y} + c_{66} \frac{\partial^2 v}{\partial x^2} + c_{22} \frac{\partial^2 v}{\partial y^2} + c_{44} \frac{\partial^2 v}{\partial z^2} + (c_{23} + c_{44}) \frac{\partial^2 w}{\partial y \partial z} = 0,$$

(1b)

$$(c_{13} + c_{55}) \frac{\partial^2 u}{\partial x \partial z} + (c_{23} + c_{44}) \frac{\partial^2 v}{\partial y \partial z} + c_{55} \frac{\partial^2 w}{\partial x^2} + c_{44} \frac{\partial^2 w}{\partial y^2} + c_{33} \frac{\partial^2 w}{\partial z^2} = 0,$$

(1c)

where c_{ij}, $i, j = 1, \ldots, 6$, denotes the elastic stiffness constants of an anisotropic plate, given in the form:

$$\begin{Bmatrix} \sigma_x \\ \sigma_y \\ \sigma_z \\ \tau_{yz} \\ \tau_{xz} \\ \tau_{xy} \end{Bmatrix} = \begin{bmatrix} c_{11} & c_{12} & c_{13} & 0 & 0 & 0 \\ c_{12} & c_{22} & c_{23} & 0 & 0 & 0 \\ c_{13} & c_{23} & c_{33} & 0 & 0 & 0 \\ 0 & 0 & 0 & c_{44} & 0 & 0 \\ 0 & 0 & 0 & 0 & c_{55} & 0 \\ 0 & 0 & 0 & 0 & 0 & c_{66} \end{bmatrix} \begin{Bmatrix} \varepsilon_x \\ \varepsilon_y \\ \varepsilon_z \\ \gamma_{yz} \\ \gamma_{xz} \\ \gamma_{xy} \end{Bmatrix}.$$

(2)

In Eq. (2), σ_x, σ_y and σ_z represent the normal stresses, while τ_{yz}, τ_{xz} and τ_{xy} denote the shear stresses. ε_x, ε_y and ε_z are the normal strains, while γ_{yz}, γ_{xz} and γ_{xy} represent shear strains. The boundary conditions include those at the plate faces and crack/anticrack-side surfaces. The three boundary conditions imposed on the plate faces, $z = \pm h$, are given as follows:

(i) Stress-free [10,11]:

$$\tau_{xz} = \tau_{yz} = \sigma_z = 0,$$

(3a)

(ii) Fixed:

$$u = v = w = 0,$$

(3b)

(iii) Lubricated

$$\tau_{xz} = \tau_{yz} = w = 0.$$

(3c)

The boundary conditions at the crack or anticrack-side surfaces are more conveniently expressed in local cylindrical polar coordinates (Figs. 1–3), which are given as follows:

(i) Crack (Fig. 1):

$$\sigma_\theta = \tau_{r\theta} = \tau_{\theta z} = 0, \quad \theta = \pm \pi$$

(4)

(ii) Anticrack (Fig. 2):

$$u_r = u_\theta = w = 0, \quad \theta = \pm \pi$$

(5)

(iii) Transversely rigid inclusion [11] (longitudinal slip permitted):

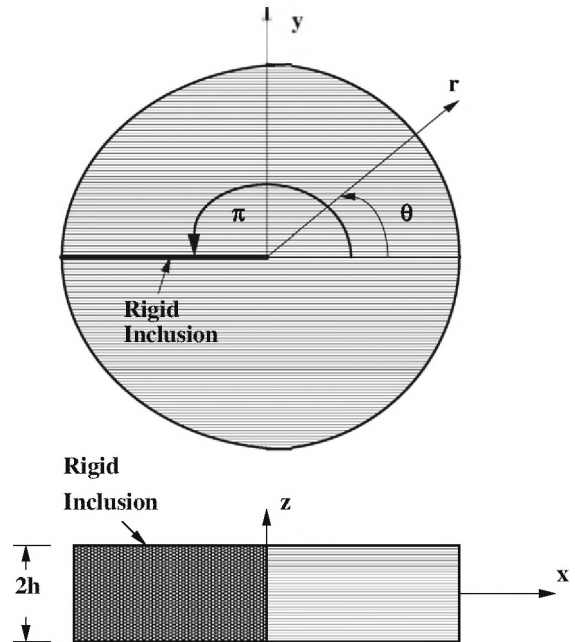$$u_\theta = \tau_{r\theta} = w = 0, \quad \theta = \pm \pi$$

(6)

Fig. 2. A through-thickness semi-infinite anticrack or perfectly bonded rigid planar inclusion in an orthotropic plate.
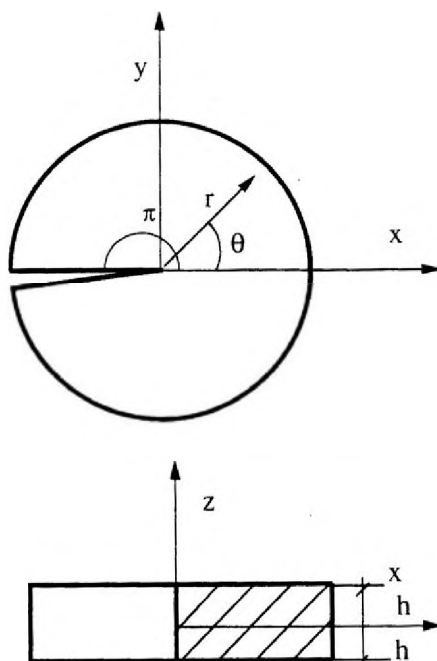

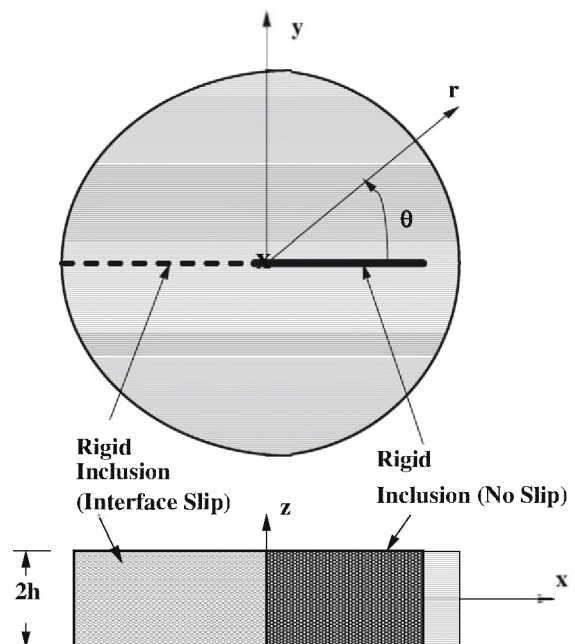**Fig. 1.** Schematic of a through-thickness semi-infinite crack in an orthotropic plate.

Fig. 3. A through-thickness semi-infinite rigid inclusion, in part perfectly bonded, the remainder with slip, in an orthotropic plate.

(iv) Rigid inclusion in part perfectly bonded, the remainder with slip [11] (Fig. 3):

$$u_\theta = u_r = w = 0, \quad \theta = 0 \tag{7a}$$

$$u_\theta = \tau_{r\theta} = \tau_{\theta z} = 0, \quad \theta = \pm\pi \tag{7b}$$

(v) Mixed or rigid inclusion alongside a crack [11]:

$$\sigma_\theta = \tau_{r\theta} = \tau_{\theta z} = 0, \quad \theta = -\pi \tag{8a}$$

$$u_r = u_\theta = w = 0, \quad \theta = \pi \tag{8b}$$

where u_r and u_θ represent the components of the displacement in r and θ directions, respectively. σ_r, σ_θ, σ_z represent the normal stresses, and $\tau_{r\theta}$, τ_{rz}, $\tau_{\theta z}$ denote the shear stresses, while ε_r, ε_θ, ε_z denote normal strains, and $\gamma_{r\theta}$, γ_{rz}, $\gamma_{\theta z}$ represent the shear strains in the cylindrical polar coordinate system (r, θ, z).

3. Singular stress fields at the front of a crack/anticrack subjected to anti-plane shear loading

The assumed displacement functions for the three-dimensional crack/anticrack problem under consideration are selected on the basis of separation of z-variables. These are as given below [28]:

$$u(x, y, z) = e^{ikz} U(x, y), \tag{9a}$$

$$v(x, y, z) = e^{ikz} V(x, y), \tag{9b}$$

$$w(x, y, z) = e^{ikz} W(x, y). \tag{9c}$$

It may be noted that since the z-dependent term and its first partial derivative can either be bounded and integrable at most admitting ordinary discontinuities, or the first partial derivative at worst be square integrable (in the sense of Lebesgue integration) in its interval $z \in [-h, h]$, i.e., admitting singularities weaker than square root (i.e., $z^{(-1/2+\varepsilon)}$, $\varepsilon > 0$), it can be best represented by Fourier series [28–30]. The latter case is justified by the Riesz–Fischer theorem [31], and its physical implication is that of satisfying the criterion of finiteness of local strain energy and path independence [32]. Substitution of Eq. (9) into Eq. (1) yields the following system of coupled partial differential equations (PDE's):

$$c_{11}\frac{\partial^2 U}{\partial x_1^2} + c_{66}\frac{\partial^2 U}{\partial y_1^2} + c_{55}U + (c_{12} + c_{66})\frac{\partial^2 V}{\partial x_1 \partial y_1} + (c_{13} + c_{55})\frac{\partial W}{\partial x_1} = 0, \tag{10a}$$

$$(c_{12} + c_{66})\frac{\partial^2 U}{\partial x_1 \partial y_1} + c_{66}\frac{\partial^2 V}{\partial x_1^2} + c_{22}\frac{\partial^2 V}{\partial y_1^2} + c_{44}V + (c_{23} + c_{44})\frac{\partial W}{\partial y_1} = 0, \tag{10b}$$

$$(c_{13} + c_{55})\frac{\partial U}{\partial x_1} + (c_{23} + c_{44})\frac{\partial V}{\partial y_1} + c_{55}\frac{\partial^2 W}{\partial x_1^2} + c_{44}\frac{\partial^2 W}{\partial y_1^2} + c_{33}W = 0, \tag{10c}$$

where

$$x_1 = ikx, \quad y_1 = iky. \tag{11}$$

The solution to the system of coupled partial differential equations (10), subjected to the far-field anti-plane shear loading, can now be sought in the form of the following modified Frobenius type series in terms of the variable $x_1 + py_1$ as follows [28], although unlike in the case of isotropic materials [10–22], the x_1 and y_1 variables are no longer separable:

$$U(x_1, y_1) = \sum_{n=0}^{\infty} a_{s+n}(x_1 + py_1)^{s+2n+1}, \tag{12a}$$

$$V(x_1, y_1) = \sum_{n=0}^{\infty} b_{s+n}(x_1 + py_1)^{s+2n+1}, \tag{12b}$$

$$W(x_1, y_1) = \sum_{n=0}^{\infty} c_{s+n}(x_1 + py_1)^{s+2n}. \tag{12c}$$

Here, the combined variable $x_1 + py_1$ represents an affine transformation in the same spirit as that by Eshelby et al. [33] and Stroh [1], although these latter authors have employed completely different techniques. Substitution of Eqs. (12) into Eqs. (10a,b) and equating the coefficients of $(x_1 + py_1)^{s+2n-1}$ yields the following recurrent relationships:

$$(s + 2n + 1)(s + 2n)(c_{11} + c_{66}p^2)a_{s+n} + c_{55}a_{s+n-1}$$
$$+ (s + 2n + 1)(s + 2n)(c_{12} + c_{66})pb_{s+n}$$
$$+ (s + 2n)(c_{13} + c_{55})c_{s+n} = 0, \tag{13a}$$

$$(s + 2n + 1)(s + 2n)(c_{12} + c_{66})pa_{s+n}$$
$$+ (s + 2n + 1)(s + 2n)(c_{22} + c_{66}p^2)b_{s+n} + c_{44}b_{s+n-1}$$
$$+ (s + 2n)(c_{23} + c_{44})c_{s+n} = 0. \tag{13b}$$

Likewise, substitution of Eq. (12) into Eq. (10c) and equating the coefficients of $(x_1 + py_1)^{s+2n-2}$ yields the following recurrent relationship:

$$(c_{13} + c_{55})a_{s+n-1} + (c_{23} + c_{44})pb_{s+n}$$
$$+ (s + 2n)(s + 2n - 1)\{c_{55} + c_{44}p^2\}c_{s+n} + c_{33}c_{s+n-1} = 0. \tag{13c}$$

For $n = 0$, Eqs. (13a–c) reduce to the following algebraic equations:

$$(s + 1)(c_{11} + c_{66}p^2)a_s + (s + 1)(c_{12} + c_{66})pb_s + (c_{13} + c_{55})c_s = 0, \tag{14a}$$

$$(s + 1)(c_{12} + c_{66})pa_s + (s + 1)(c_{22} + c_{66}p^2)b_s + (c_{23} + c_{44})c_s = 0, \tag{14b}$$

for $s \neq 0$, $s \neq -1$;

$$\{c_{55} + c_{44}p^2\}c_s = 0, \quad \text{for} \quad s \neq 0, \ s \neq 1; \tag{14c}$$

since

$$a_{s-1} = b_{s-1} = c_{s-1} = 0.$$

For nontrivial c_s, Eq. (14c) supplies the following characteristic equation

$$c_{55} + c_{44}p^2 = 0, \tag{15a}$$

leading to

$$p_{1,2} = \pm i\sqrt{\frac{c_{55}}{c_{44}}}. \tag{15b}$$

In addition, since a z-dependent term is, as mentioned earlier, assumed in the form of a Fourier series, the assumed displacement functions can be written as follows:

$$w(x, y, z) = \{\overline{D}_1 \cos(kz) + \overline{D}_2 i \sin(kz)\}$$
$$\times (ik)^s \left[\overline{C}_1\left(x + i\sqrt{\frac{c_{55}}{c_{44}}}y\right)^s + \overline{C}_2\left(x - i\sqrt{\frac{c_{55}}{c_{44}}}y\right)^s\right], \tag{16a}$$

$$u(x, y, z) = \{\overline{D}_1 i \sin(kz) + \overline{D}_2 \cos(kz)\}$$
$$\times (ik)^{s+1} \left[\overline{A}_1\left(x + i\sqrt{\frac{c_{55}}{c_{44}}}y\right)^{s+1} + \overline{A}_2\left(x - i\sqrt{\frac{c_{55}}{c_{44}}}y\right)^{s+1}\right], \tag{16b}$$

$$v(x,y,z) = \{\overline{D}_1 i \sin(kz) + \overline{D}_2 \cos(kz)\}$$

$$\times (ik)^{s+1} \left[\overline{B}_1 \left(x + i\sqrt{\frac{c_{55}}{c_{44}}}y \right)^{s+1} + \overline{B}_2 \left(x - i\sqrt{\frac{c_{55}}{c_{44}}}y \right)^{s+1} \right]. \tag{16c}$$

It is convenient to express the components of displacements and stresses in terms of cylindrical polar coordinates. The general asymptotic form for the displacement components can be written as follows:

$$w(r,\theta,z) = r^s B_b(z) \left[\cos^2(\theta) + \frac{c_{55}}{c_{44}} \sin^2(\theta) \right]^{s/2} [C_1 \cos(s\phi)$$
$$+ C_2 \sin(s\phi)] + O(r^{s+2}), \tag{17a}$$

$$u_r(r,\theta,z) = O(r^{s-1}), \quad u_\theta(r,\theta,z) = O(r^{s-1}), \tag{17b}$$

where

$$\phi = \tan^{-1}\left(\sqrt{\frac{c_{55}}{c_{44}}} \tan(\theta) \right), \tag{18}$$

$$C_1 = \overline{C}_1 + \overline{C}_2, \tag{19a}$$
$$C_2 = i(\overline{C}_1 + \overline{C}_2), \tag{19b}$$

and

$$B_b(z) = -D_1 \cos(kz) + D_2 \sin(kz), \tag{20}$$

in which

$$D_1 = -(ik)^s \overline{D}_1, \quad D_2 = i(ik)^s \overline{D}_2, \tag{21}$$

wherein k is an integer. The singular stress field can be obtained from Eqs. (16) or (17) as follows:

$$\tau_{\theta z}(r,\theta,z) = c_{44} r^{s-1} B_b(z) s \left\{ \cos^2(\theta) + \frac{c_{55}}{c_{44}} \sin^2(\theta) \right\}^{(s-1)/2}$$
$$\times \left\{ \frac{c_{55}}{c_{44}} \cos^2(\theta) + \sin^2(\theta) \right\}^{1/2}$$
$$\cdot \{ C_1 \cos(s\phi + \phi' - \phi) + C_2 \sin(s\phi + \phi' - \phi) \} + O(r^{s-1}), \tag{22a}$$

$$\tau_{rz}(r,\theta,z) = c_{55} r^{s-1} B_b(z) s \left\{ \cos^2(\theta) + \frac{c_{55}}{c_{44}} \sin^2(\theta) \right\}^{s/2}$$
$$\times \{ C_1 \cos(s\phi) + C_2 \sin(s\phi) \} + O(r^{s-1}), \tag{22b}$$

$$\tau_{r\theta} = O(r^s), \quad \sigma_r = O(r^s), \tag{22c, d}$$

$$\sigma_\theta = O(r^s), \quad \sigma_z = O(r^s), \tag{22e, f}$$

where

$$\phi' = \tan^{-1}\left(-\sqrt{\frac{c_{55}}{c_{44}}} \cot(\theta) \right). \tag{23}$$

For an isotropic or cubic single crystal material, $c_{55} = c_{44}$, and Eqs. (18) and (23) reduce to

$$\phi = \theta, \tag{24a}$$
$$\phi' = \frac{\pi}{2} + \theta. \tag{24b}$$

It may be noted that since s or $Re\,s$ (when s is complex) is positive, all the higher order terms in Eqs. (22) vanish as $r \to 0$.

3.1. Plate surface boundary conditions

(i) Satisfaction of stress-free boundary conditions, given by Eq. (3a), on the plate faces results in:

$$B_b(\pm h) = B_{bs}(\pm h) + B_{ba}(\pm h) = 0, \tag{25}$$

where

$$B_{bs}(\pm h) = -D_1 \cos(\pm kh), \tag{26a}$$
$$B_{ba}(\pm h) = D_2 \sin(\pm kh). \tag{26b}$$

The special case of symmetric deformation is obtained as follows:

$$D_2 = 0, \tag{27}$$

$$k_m = \frac{(2m+1)\pi}{2h}, \quad m = 1,2,\dots, \tag{28a}$$

which, on substitution into Eq. (20), yields

$$B_{bs}(z) = -\sum_{m=0}^{\pm\infty} D_{1m} \cos\left(\frac{(2m+1)\pi z}{2h} \right). \tag{28b}$$

The antisymmetric deformation case can also be obtained in a similar manner, as given below:

$$D_1 = 0, \tag{29}$$

$$k_m = \frac{m\pi}{h}, \quad m = 1,2,\dots, \tag{30a}$$

$$B_{ba}(z) = \sum_{m=0}^{\pm\infty} D_{2m} \sin\left(\frac{m\pi z}{h} \right). \tag{30b}$$

(ii, iii) Satisfaction of fixed and lubricated boundary conditions, given by Eqs. (3b) and (3c), respectively, on the plate faces results in identical expressions for the displacement and singular stress fields as above.

3.2. Crack/anticrack side boundary conditions

The expressions for stresses and displacements also need to satisfy the boundary conditions on the crack, anticrack or mixed crack-anticrack-side surfaces.

3.2.1. Crack
Substitution of Eq. (22a) into Eq. (4) yields the characteristic equation for a crack:

$$\sin(2s\pi) = 0. \tag{31}$$

The minimum root (eigenvalue), contributing to the singular stress field, is given by $s = 1/2$, which is the same as that for its isotropic plate counterpart [10]. It must be stressed that strength of the stress singularity remains unchanged throughout the plate thickness. The stress distribution in the vicinity of a semi-infinite crack front can now be expressed as follows:

$$\tau_{rz}(r,\theta,z) = \frac{K_{III}(z)}{\sqrt{2\pi r}} \frac{c_{55}}{c_{44}} \left\{ \cos^2\theta + \frac{c_{55}}{c_{44}} \sin^2\theta \right\}^{1/2} \sin\left(\frac{\phi}{2} \right), \tag{32a}$$

$$\tau_{\theta z}(r,\theta,z) = \frac{K_{III}(z)}{\sqrt{2\pi r}} \left\{ \frac{c_{55} \cos^2\theta + c_{44} \sin^2\theta}{c_{44} \cos^2\theta + c_{55} \sin^2\theta} \right\}^{1/2} \sin\left(\phi' - \frac{\phi}{2} \right), \tag{32b}$$

while the transverse displacement component is given by

$$w(r,\theta,z) = \frac{2K_{III}(z)}{c_{44}} \sqrt{\frac{r}{2\pi}} \left\{ \cos^2\theta + \frac{c_{55}}{c_{44}} \sin^2\theta \right\}^{1/2} \sin\left(\frac{\phi}{2} \right), \tag{33}$$

where

$$\sin\left(\frac{\phi}{2} \right) = \sqrt{\frac{1}{2}} \left[1 - \left(\frac{c_{44} \cos^2\theta}{c_{44} \cos^2\theta + c_{55} \sin^2\theta} \right)^{1/2} \right]^{1/2}, \tag{34a}$$

$$\cos\left(\frac{\phi}{2} \right) = \sqrt{\frac{1}{2}} \left[1 + \left(\frac{c_{44} \cos^2\theta}{c_{44} \cos^2\theta + c_{55} \sin^2\theta} \right)^{1/2} \right]^{1/2}, \tag{34b}$$

$$\sin(\phi') = \left(\frac{c_{55}}{c_{44} \cos^2\theta + c_{55} \sin^2\theta} \right)^{1/2} \cos\theta. \tag{34c}$$

The above results reduce to their isotropic [10] and cubic single crystal [28] counterparts by virtue of Eqs. (24). $K_{III}(z)$, which denotes the stress intensity factor, can be split into symmetric and antisymmetric parts (with respect to z):

$$K_{III}(z) = K_{IIIs}(z) + K_{IIIa}(z), \tag{35}$$

with

$$K_{IIIs} = \sqrt{\frac{\pi}{2}} c_{44} C_2 B_{bs}(z), \tag{36a}$$

$$K_{IIIa} = \sqrt{\frac{\pi}{2}} c_{44} C_2 B_{ba}(z). \tag{36b}$$

C_2 is a constant. It is clear that

$$\int_{-h}^{h} K_{IIIa} dz = 0. \tag{37}$$

K_{IIIa} thus obtained represents the self-equilibrating stress intensity factor for a semi-infinite crack, resulting in the residual stresses in the orthotropic plate material. It must be noted that K_{IIIa} cannot be determined by a two-dimensional approximation, which yields constant K_{IIIs}, while both K_{IIIa} and K_{IIIs}, derived by the above three-dimensional approach, are functions of z.

Figs. 4 and 5 show variations of the normalized stress intensity factor, $K^*(z) = K(z)/K_{AntiplaneShear(2D)}$, through the normalized thickness coordinate, $z^* = z/h$, of an orthotropic plate and weakened by a through-crack investigated here. For an infinite cylindrical shaped body with a center-crack of length $2a$, $K_{AntiplaneShear(2D)}$ was first given by Sih et al. [2] as $\tau_{Antiplane}^\infty \sqrt{a}$, where $\tau_{Antiplane}^\infty$ is the applied far-field loading. This definition of K has been modified with a multiplying factor of $Y = \sqrt{\pi}$, with the result that $K_{AntiplaneShear(2D)} = \sqrt{\pi} \tau_{Antiplane}^\infty \sqrt{a}$. Fig. 4 shows the through-thickness variation of the stress intensity factor for a far-field anti-plane shear (mode III) load, while its antisymmetric counterpart respon-

Fig. 4. Variation of stress intensity factor for anti-plane shear loading through thickness.

Fig. 5. Variation of stress intensity factor for singular residual stress through thickness.

sible for singular residual stress field is displayed in Fig. 5. The latter types of results are, to this date, unavailable in the literature. It may be noted that the applied far-field anti-plane shear stress considered here is constant through the plate thickness. For a two-dimensional LEFM analysis, such as that due to Sih et al. [2], this is not an issue, since there are no boundary conditions that need to be satisfied at the top and bottom surfaces of the plate, $z^* = \pm1$. However, for a three-dimensional LEFM analysis carried out in the present study, a great complication arises in terms of through-thickness constant applied (far-field) stress, $\tau_{Antiplane}^\infty$, and satisfying the boundary conditions at $z^* = \pm1$. These conflicting goals are reconciled in the present analysis, by employing a large number of terms (about 300,000) in order to replicate the sharp drop to zero at the top and bottom (stress free) surfaces of the cracked orthotropic plate under investigation. This is clearly shown in Fig. 6.

3.2.2. Anticrack

Substitution of Eq. (17a) into Eq. (5) yields the characteristic equation for an anticrack:

$$\sin(2s\pi) = 0. \tag{38}$$

The minimum root (eigenvalue), contributing to the singular stress field, is given by $s = 1/2$, which is the same as that for its isotropic plate counterpart [11]. The stress distribution in the vicinity of a semi-infinite anticrack front can now be expressed as follows:

$$\tau_{rz}(r, \theta, z) = \frac{S_{III}(z)}{\sqrt{2\pi r}} \frac{c_{55}}{c_{44}} \left(\cos^2\theta + \frac{c_{55}}{c_{44}} \sin^2\theta \right)^{1/2} \cos\left(\frac{\phi}{2}\right), \tag{39a}$$

$$\tau_{\theta z}(r, \theta, z) = \frac{S_{III}(z)}{\sqrt{2\pi r}} \left(\frac{c_{55}\cos^2\theta + c_{44}\sin^2\theta}{c_{44}\cos^2\theta + c_{55}\sin^2\theta} \right)^{1/2} \cos\left(\phi' - \frac{\phi}{2}\right), \tag{39b}$$

while the transverse displacement component is given by

$$w(r, \theta, z) = \frac{2S_{III}(z)}{c_{44}} \sqrt{\frac{r}{2\pi}} \left(\cos^2\theta + \frac{c_{55}}{c_{44}} \sin^2\theta \right)^{1/2} \cos\left(\frac{\phi}{2}\right). \tag{40}$$

The above results reduce to their isotropic [11] counterparts by virtue of Eqs. (24). $S_{III}(z)$, known as the stress singularity coefficient [3], is also a function of z, and can be split into symmetric and antisymmetric parts (with respect to z):

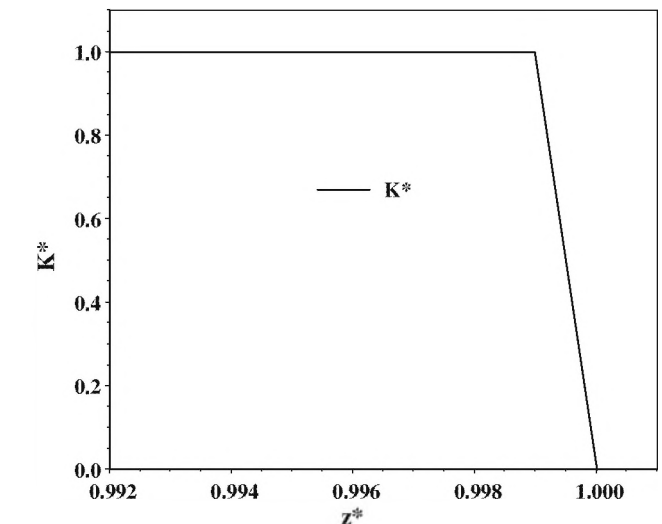$$S_{III}(z) = S_{IIIs}(z) + S_{IIIa}(z), \tag{41}$$
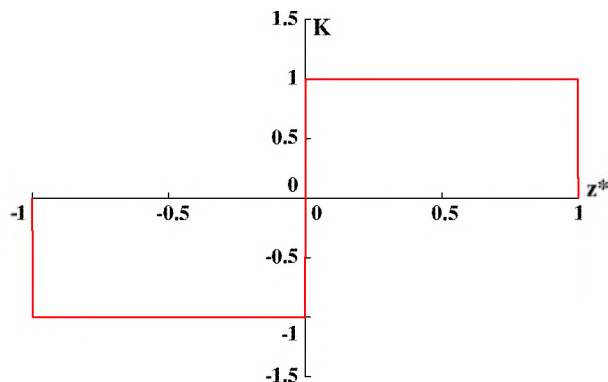
Fig. 6. Sharp drop of stress intensity factor to zero in the vicinity of the top surface of a cracked plate for constant-through-thickness far-field loading.

with

$$S_{IIIs} = \sqrt{\frac{\pi}{2}} c_{44} C_1 B_{bs}(z), \tag{42a}$$

$$S_{IIIa} = \sqrt{\frac{\pi}{2}} c_{44} C_1 B_{ba}(z). \tag{42b}$$

C_1 is a constant. It is clear that

$$\int_{-\hbar}^{\hbar} S_{IIIa} dz = 0. \tag{43}$$

S_{IIIa} thus obtained represents the self-equilibrating stress singularity coefficient for a semi-infinite anticrack, resulting in the residual stresses in the material. It must be noted that S_{IIIa} cannot be determined by a two-dimensional approximation, which yields constant S_{IIIs}, while both S_{IIIa} and S_{IIIs}, obtained by the above three-dimensional approach, are functions of z. Through-thickness variations of these stress singularity coefficients can be represented in a manner similar to their stress intensity factor counterparts as shown in Figs. 4 and 5.

3.2.3. Transversely rigid inclusion (longitudinal slip permitted)

Substitution of Eq. (17a) into Eq. (6) supplies the same characteristic equation as in the case of an anticrack. Since $\tau_{r\theta} = O(r^s)$, i.e., $\tau_{r\theta}$ is nonsingular and the only boundary condition that determines the lowest eigenvalue, s, is given by $w = 0$, at $\theta = \pm\pi$, this situation is identical to that of case 3.2.2. The mode III stress singularity coefficients are also identical, and will not be repeated here.

3.2.4. Rigid inclusion in part perfectly bonded, the remainder with slip

Substitution of Eq. (22a) into Eq. (7b) supplies the same characteristic equation as in the case of a through crack. It may be noted here that the interface continuity condition, given by Eq. (7a) is automatically satisfied. Furthermore, the only boundary condition that determines the lowest eigenvalue, s, is given by $\tau_{\theta z} = 0$, at $\theta = \pm\pi$. Consequently, this situation is identical to that of case 3.2.1. The mode III stress intensity factors are also identical to their counterparts for a crack, and will not be repeated here.

3.2.5. Rigid inclusion alongside crack

Lastly, substitution of Eq. (22a) into Eq. (8a), and that of Eq. (17a) into Eq. (8b) yields the characteristic equation for a mixed crack/anticrack:

$$\cos(2s\pi) = 0. \tag{43}$$

The two lowest roots (eigenvalues), contributing to the singular stress field, is given by $s = 1/4$, $s' = 3/4$, which are identical to their isotropic plate counterpart [11]. The singular parts of τ_{rz} and $\tau_{\theta z}$ are given as follows:

$$\tau_{rz}, \quad \tau_{\theta z} \sim O(r^{-3/4}) + O(r^{-1/4}). \tag{44}$$

4. Summary, discussions and conclusions

A heretofore-unavailable eigenfunction expansion technique, based partly on separation of the z-variable and in part, on the Eshelby et al. [33] and Stroh [1] type affine transformation, is developed to derive three-dimensional asymptotic displacement and stress fields in the vicinity of the front of a semi-infinite through-thickness crack/anticrack weakening/reinforcing an infinite orthotropic/orthorhombic plate. Crack, anticrack or mixed crack-anticrack-face boundary conditions and those that are prescribed on the top and bottom (free, fixed and lubricated) surfaces of the orthotropic plate are exactly satisfied. Five different through-thickness crack/anticrack-face boundary conditions are considered: (i) slit crack, (ii) anticrack or perfectly bonded rigid inclusion, (iii) transversely rigid inclusion (longitudinal slip permitted), (iv) rigid inclusion in part perfectly bonded, the remainder with slip, and (v) rigid inclusion located alongside a crack. Explicit expressions for the singular stress fields in the vicinity of the fronts of the through-thickness cracks, anticracks or mixed crack-anticrack type discontinuities, weakening/reinforcing orthotropic/orthorhombic plates, subjected to far-field anti-plane shear (mode III) loadings, are presented.

Among interesting conclusions of the present investigation, K_{IIIa} and S_{IIIa}, obtained here represent the self-equilibrating stress intensity factor and stress singularity coefficient, respectively, for a semi-infinite through-thickness crack/anticrack, resulting in residual stresses in the orthotropic plate material. It must be recognized that K_{IIIa} (or S_{IIIa}) cannot be determined by a two-dimensional approach, which yields constant K_{IIIs} (or S_{IIIs}), while both K_{IIIa} (or S_{IIIa}) and K_{IIIs} (or S_{IIIs}), obtained by the above three-dimensional approach, are functions of z.

The singular residual stress in a monocrystalline orthorhombic (cubic as a special case) material appears to be screw dislocation-like. This can be interpreted as the core of a screw dislocation getting trapped at the crack front. For example, since for (cubic) monocrystalline silicon, the room temperature is much lower than what is needed for brittle-to-ductile transition, such trapped screw dislocation core would not be able to induce large scale plasticity in its neighborhood. It should be possible to measure the out of plane displacement component, w, by cutting a cylindrical piece of solid radially (see e.g., Fig. 2.14 of Hertzberg [5]). The plate material undergoes high shear deformation in the vicinity of a crack or anticrack in the r–z plane (θ normal), and r–θ plane (z normal) which may cause high shear distortion in the lattice, resulting in both bond scission and bond rotation.

In a fiber reinforced composite material, the singular residual stress field can be high enough to cause cracking within the matrix. This micro-cracking of the matrix can expose the fibers to degradation by chemical attack [8]. In addition, the fibers may themselves be sheared by the action of such high $\tau_{\theta z}$ and τ_{rz} gradient, especially in the presence of out-of-plane waviness of fibers.

References

[1] Stroh AN. Dislocations and cracks in anisotropic elasticity. Philos Mag 1958;7:625–46.

[2] Sih GC, Paris PC, Irwin GR. On cracks in rectilinear anisotropic bodies. Int J Fract Mech 1965;1:189–203.

[3] Wang ZY, Zhang HT, Chou YT. Characteristics of the elastic field of a rigid line inhomogeneity. ASME J Appl Mech 1985;52:818–22.

[4] Chaudhuri RA, Xie M, Garala HJ. Stress singularity due to kink band weakening a unidirectional composite under compression. J Compos Mater 1996;30:672–91.

[5] Hertzberg RW. Deformation and fracture mechanics of engineering materials. 4th ed. New York: John Wiley & Sons; 1996.

[6] Cook RF, Dinger TR, Clarke DR. Fracture toughness measurements of YBa₂Cu₃Oₓ single crystals. Appl Phys Lett 1987;61:454–6.

[7] Vrinceanu ID, Danyluk S. Measurement of residual stress in single crystal silicon wafers. In: Proceedings of 8th int. symp. adv. packaging mater, Stone Mountain, GA (USA); March 2002.

[8] White SR, Hahn HT. Process modeling of composite materials: residual stress development during cure. Part I. model formulation. J Compos Mater 1992;26:2402–22.

[9] Stenger F, Chaudhuri R, Chiu J. Sinc solution of boundary integral form for two-dimensional bi-material elasticity problems. Compos Sci Technol 2000;60:2197–211.

[10] Chaudhuri RA, Xie M. A novel eigenfunction expansion solution for three-dimensional crack problems. Compos Sci Technol 2000;60:2565–80.

[11] Chaudhuri RA. Eigenfunction expansion solutions for three-dimensional rigid planar inclusion problem. Int J Fract 2003;121:95–110.

[12] Chaudhuri RA, Xie M. A tale of two saints: St. Venant and "St. Nick" — does St. Venant's principle apply to bimaterial straight edge and wedge singularity problems? Compos Sci Technol 2000;60:2503–15.

[13] Xie M, Chaudhuri RA. Three-dimensional stress singularity at a bimaterial interface crack front. Compos Struct 1998;40:137–47.

[14] Chaudhuri RA, Xie M. Free-edge stress singularity in a bimaterial laminate. Compos Struct 1998;40:129–36.

[15] Chaudhuri RA. Three-dimensional asymptotic stress field in the vicinity of the circumference of a penny shaped discontinuity. Int J Solids Struct 2003;40:3787–805.

[16] Chaudhuri RA. Three-dimensional asymptotic stress field in the vicinity of the circumference of a bimaterial penny shaped interface discontinuity. Int J Fract 2006;141:207–21.

[17] Chaudhuri RA. Three-dimensional singular stress field near a partially debonded cylindrical rigid fiber. Compos Struct 2006;72:141–50.

[18] Chaudhuri RA. Three-dimensional asymptotic stress field in the vicinity of the circumferential tip of a fiber-matrix interfacial debond. Int J Eng Sci 2004;42:1707–27.

[19] Chaudhuri SN, Chaudhuri RA, Benner RE, Penugonda M. Raman spectroscopy for characterization of interfacial debonds between carbon fibers and polymer matrices. Compos Struct 2006;76:375–87.

[20] Chaudhuri RA. Three-dimensional asymptotic stress field in the vicinity of the line of intersection of a circular cylindrical through/part-through open/rigidly plugged hole and a plate. Int J Fract 2003;122:65–88.

[21] Chaudhuri RA. Three-dimensional asymptotic stress field in the vicinity of the line of intersection of an inclusion and plate surface. Int J Fract 2003;117:207–33.

[22] Chaudhuri RA. An eigenfunction expansion solution for three-dimensional stress field in the vicinity of the circumferential line of intersection of a bimaterial interface and a hole. Int J Fract 2004;129:361–84.

[23] Folias ES. On interlaminar stresses of a composite plate around the neighborhood of a hole. Int J Solids Struct 1989;25:1193–200.

[24] Ma CC, Hour BL. Antiplane problems in composite anisotropic materials with an inclined crack terminating at a bimaterial interface. Int J Solids Struct 1990;26:1387–400.

[25] Xie M, Chaudhuri RA. Three-dimensional asymptotic stress field at the front of a bimaterial wedge of symmetric geometry under antiplane shear loading. Compos Struct 2001;54:509–14.

[26] Chiu JSH, Chaudhuri RA. Three-dimensional asymptotic stress field at the front of an unsymmetric bimaterial pie-shaped wedge under antiplane shear loading. Compos Struct 2002;58:129–37.

[27] Nye JF. Physical properties of crystals. Oxford: Oxford University Press; 1979.

[28] Chaudhuri RA. Three-dimensional singular stress field at the front of a crack and lattice crack deviation in a cubic single crystal plate. Philos Mag; in press.

[29] Chaudhuri RA, Chiu SHJ. Three-dimensional asymptotic stress field at the front of an unsymmetric bimaterial wedge associated with matrix cracking or fiber break. Compos Struct 2007;78:254–63.

[30] Chaudhuri RA, Chiu SHJ. Three-dimensional asymptotic stress field in the vicinity of an adhesively bonded scarf joint interface. Compos Struct 2009;89:475–83.

[31] Carslaw HS. Introduction to the theory of Fourier series and integrals. 3rd ed. New York: Dover; 1930.

[32] Wilcox CH. Uniqueness theorems for displacement fields with locally finite energy in linear elastostatics. J Elast 1979;9:221–43.

[33] Eshelby JD, Read WT, Shockley W. Anisotropic elasticity with application to dislocation theory. Acta Metall 1953;1:251–9.